Impurity dimers in superconducting B-doped diamond: Experiment and first-principles calculations

E. Bourgeois,[1] E. Bustarret,[2] P. Achatz,[2,3] F. Omnès,[2] and X. Blase[1]
[1]*Laboratoire de Physique de la Matière Condensée et des Nanostructures, Université Lyon I, CNRS, UMR 5586, Domaine Scientifique de la Doua, F-69622 Villeurbanne Cedex, France*
[2]*Laboratoire d'Etude des Propriétés Electroniques des Solides, CNRS Boîte Postal 38042, Grenoble Cedex 09, France*
[3]*CEA/DRFMC/SPSMS, 17 Avenue des Martyrs, 38054 Grenoble Cedex 9, France*
(Received 18 May 2006; revised manuscript received 25 July 2006; published 20 September 2006)

On the basis of first-principles calculations and experimental secondary ion mass spectroscopy, electrical transport, and Raman measurements performed on homoepitaxial diamond, we find that at high concentrations boron atoms tend to segregate in dimers. The study of the electronic, vibrational, and electron-phonon coupling properties, corroborated by Raman measurements, shows that boron dimers may be associated to the broad Raman peak around 500 cm^{-1} as well as to some of the gap states which have been reported in the literature, and that they are both electrically and vibrationally inactive with respect to the electron-phonon coupling driving the superconducting transition in metallic diamond. These results bear important consequences on the evolution of the critical temperature with the impurity concentration in B-doped diamond.

DOI: 10.1103/PhysRevB.74.094509 PACS number(s): 74.62.Bf, 71.15.Mb, 74.20.Fg, 74.25.Kc

I. INTRODUCTION

A few decades after early discussions on the superconducting transition in semiconductors,[1] the experimental discovery of superconductivity in heavily boron-doped diamond triggered much experimental[2–13] and theoretical[14–19] activity to confirm, study, and understand the observed superconducting transition. The experimental critical temperature transition T_C was found to depend on the impurity concentration,[4,9] with a threshold boron-to-carbon atomic concentration ratio x so far indistinguishible from the critical concentration for the metal-to-insulator transition $x_c \sim 0.3$ at. % as determined in (001)-oriented epilayers,[6] while maximum T_C values on the order of 10 K have been reported.[7,9,10] However, the parameters governing the complex relationship between the boron content or the hole concentration and T_C have not yet been determined, and they are currently the object of many experimental investigations, not only near the metal to insulator transition, but also at higher concentrations. The dependence of T_C on x has been shown recently to depend on the growth direction[7] and gas mixture composition.[10] The difficulties in relating the observed T_C with boron content, which was also emphasized in Ref. 8, may result from variations in the doping efficiency of boron atoms, a feature generally ascribed to hydrogen passivation[20] or to nonsubstitutional incorporation sites. For example, in a (111)-oriented thick superconducting film with $x=5$ at. %, the free hole density was estimated[11] to take a much lower value lying in the 0.4 to 2.4% concentration range. Less than 50% dopant activation has also been reported for hydrogen-free superconducting polycrystalline diamond grown at high temperature and high pressure.[21]

Most experiments favor a standard BCS picture involving a phonon-mediated pairing mechanism, with a Fermi level well into the valence band[8,11] and a superconducting gap value, spectral shape, and temperature dependence[12] shown to be fully compatible with the BCS model, as also corroborated by recent optical measurements.[13] Such results confirm several theoretical works which, on the basis of the virtual crystal approximation (VCA)[14–16] or supercell techniques,[17,18] suggested that the standard BCS approach, where pairing results from electron-phonon interactions, was consistent with the available experimental observations. These conclusions were substantiated by previous work on similar σ-bonded systems such as MgB_2 (Ref. 22) or doped covalent clathrates[23] for which BCS was giving excellent results, as evidenced either by a direct comparison with the experimentally measured λ parameter[23] or by adopting a newly developed parameter-free approach[24] where the Coulomb repulsion parameter μ^* does not need to be adjusted.

In contrast to this, in a recent experimental work, x-ray emission and x-ray absorption (XAS) was used to explore the electronic density of states of normal and superconducting B-doped diamond samples.[25] In addition to the clear signature of the impurity band ascribed to boron in the normal state, already reported for heavily doped but nonsuperconducting films,[26] a key observation was the occurrence of deep and strongly broadened B-related unoccupied states in the energy gap of the only sample that became superconducting at low temperatures.[25] Such features had not been predicted by the above mentioned theoretical investigations, and have been considered as a support for alternative approaches involving electronic correlation effects, originating either in the proximity of dopants occupying neighboring interstitial sites[27] or in the strong electronic correlations of boron-related states leading to the properties of the resonating valence band model.[28] Finally, it has also been argued that the optical conductivity spectrum of the polished surface of a superconducting polycrystalline diamond films provided some evidence[29] for the existence of an impurity band close to the top of the valence band.

In this work, the study of the structural, electronic, and electron-phonon coupling properties in B-doped diamond will be presented, emphasizing the presence and role of boron dimers in heavily doped samples. In Sec. II, on the basis of supercell *ab initio* simulations where B atoms are allowed

to cluster, we find that boron dimers are energetically favored, in particular under hole-doping conditions. Boron dimers are shown to generate inactive in-gap states and vibrational modes in the 400–600 cm^{-1} range that do not couple to the holes at the top of the valence bands. Such results are corroborated in Sec. III by experimental results on the incorporation efficiency of boron atoms during growth and by Raman scattering measurements: the experimental spectra show a parallel-polarized broad peak around 500 cm^{-1}, within the wave number range calculated for the A_1 stretching modes of boron dimers. Contrary to the optical modes, this peak has the same line shape in superconducting and nonsuperconducting epilayers and does not show any sign of a quantum interference with the electronic light scattering by free carriers. We then discuss in Sec. IV the consequences of these results on the superconducting properties of B-doped diamond, before presenting our conclusions in Sec. V.

II. THEORETICAL STUDY

A. Technical details

In the supercell approach, impurities in the unit cell are repeated periodically, a description that may not reflect the experimental random distribution of dopants. By studying several geometries, we can, however, extract general electronic and vibrational features that are shown to strongly affect the superconducting properties. We therefore consider two different unit cells containing, respectively, 54 atoms (a $3\times3\times3$ repetition of the standard fcc 2-atom-cell lattice) and a 64-atom one built as a $2\times2\times2$ repetition of the conventional simple cubic 8-atom cell. Two to three carbon atoms were substituted by boron leading to B_nC_{54-n} or B_nC_{64-n} $(n=2,3)$ systems.

Our calculations are performed both within the local density approximation (LDA) and a gradient-corrected functional (PBE)[30] to the density functional theory,[31] implemented within a planewave pseudopotential formalism.[32] LDA calculations are performed with Troullier-Martins pseudopotential[33] and a 60 Ryd cutoff is found to give well-converged energy differences. PBE calculations are conducted using ultrasoft pseudopotentials[34] with a 30 Ryd cutoff for the eigenstates and 240 Ry for the charge density. The **k**-point sampling is increased to convergency, that is a $(4\times4\times4)$ grid for structural relaxation and phonon calculations, completed in total energy calculations by an $(8\times8\times8)$ self-consistent run for a good mapping of the Fermi surface using Methfessel-Paxton broadening. The average electron-phonon coupling, for a given phonon momentum, is achieved by sampling the Fermi surface with a $(6\times6\times6)$ **k**-point grid.

B. Structure and stability of dimers

We first minimize the energy of the system with respect to atomic positions. In the case of two impurities per cell, several relative positions are considered: first (NN), second (2NN), and third (3NN) nearest neighbors. In the case of the 3NN configurations, the two nonequivalent possible geometries are explored. The stability of these various geometries are provided in Table I. Surprisingly enough, the first nearest neighbor configuration is very stable, preferable in most situations to other configurations, both within LDA and GGA (PBE consistently favors the NN configuration as compared to LDA). Such a result contrast significantly with the case of B in bulk silicon where the NN configuration is strongly disfavored due to tensile strain.[35] Our findings confirm and extend the recent work by Goss *et al.* where the B_2C_{62}-NN configuration was found to be more stable than the B_2C_{62}-2NN one by 200 meV within a different localized-basis LDA approach.[36] In the impurity-dimer geometry, the B-B bond distance is found to be elongated by ~26% along the {111} direction preserving a local D_{3d} symmetry. The B atoms are located very close (~0.4 Å) to the plane formed by their three backbonded carbon atoms. Averaging over the different cells, the NN, 2NN, and 3NN B-B distances are 1.95, 2.48, and 3.43 Å, respectively. We finally explore a configuration where the three B atoms are clustered in the B_3C_{61} cell. Such a configuration is found to be less stable by at least ~280 meV as compared to B_3C_{61}-NN configurations comprizing a boron dimer plus an isolated boron atom.[37]

TABLE I. Relative stability (in meV) of various configurations (see text). The reference of energy is taken to be that of the nearest-neighbor configuration. A positive number means a less stable structure. In parenthesis, results for the charged defects (hole doping).

	B_2C_{52}			B_2C_{62}	
	LDA		PBE	LDA	PBE
NN	00	(00)	00	00	00
2NN	40	(150)	50	145	170
3NN-a	–45	(50)	–25	90(150)	110
3NN-b	155	(320)	170	160	205

To strengthen our conclusions, we note that we are interested in studying dopant structures in heavily *p*-doped diamond, a situation which might not be reflected by considering a distribution of neutral dimers.[38] To test the effect of hole-doping onto the energies presented in Table I, we have repeated our LDA calculations for several configurations removing an electronic charge amounting to an additional 1% doping.[39] The results are indicated in parenthesis (Table I). Very clearly, the dimer complex is strongly stabilized in a hole-doping environment and the dimer configuration is now found to be always more stable. Additional hole doping further stabilizes the dimer. This is a very strong indication that upon increasing hole doping, boron dimers will be thermodynamically favored. This enhancement of the dimer stability is mainly electronic as relaxation of the atomic positions under further hole doping hardly contributes to the evolution of the energy differences presented in the table. On the contrary, we find that adding electrons to the system (*n*-type doping) strongly destabilizes the dimer configuration.[37]

Even though the difference in energy between the dimer (or NN) and "unsegregated" configurations strongly depends on the cell size and atomic relative positions, it is clear that in the limit of large doping, impurities should be driven to

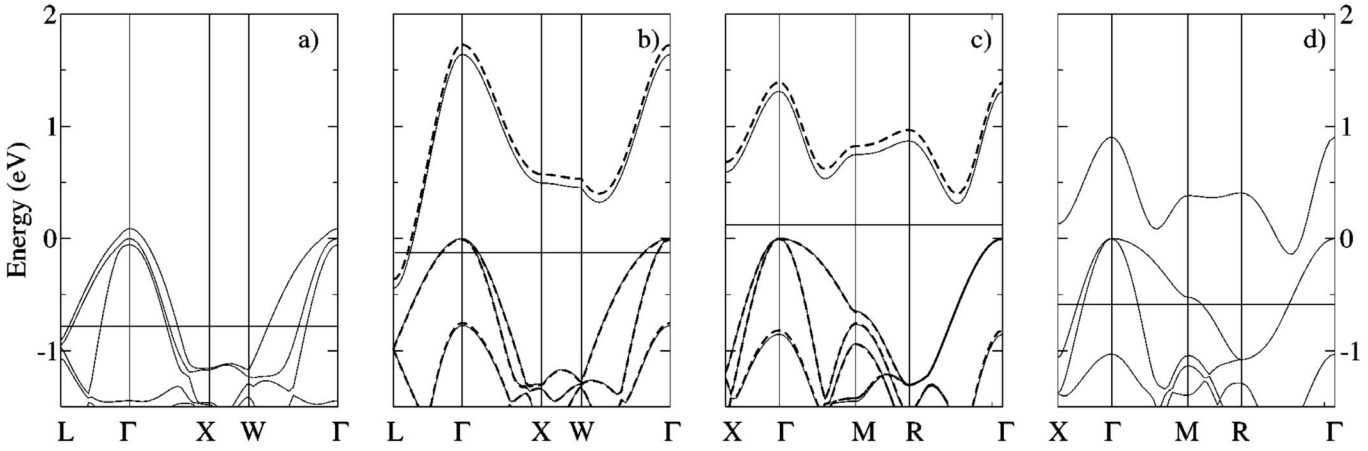

FIG. 1. Electronic band structure of the (a) B_2C_{52}-3NN-a, (b) B_2C_{52}-NN, (c) B_2C_{62}-NN, and (d) B_3C_{61}-NN cells. Horizontal lines indicate the Fermi level position. In dotted, we plot the deformation of the band structures associated with the highest energy A_{1g} B-B stretching mode (normalized displacement amplitude is so that the B-B elongation is the same in the two cells). The 3NN-a and 3NN-b configurations (see Table I) yield similar band structures. The zero of energy has been set to the VBM. The chosen B_3C_{61}-NN band structure is representative of all possible structures with one dimer plus an isolated boron atom (see Ref. 37).

the preferential formation of dimers. The large destabilization of the three B-atom cluster suggests that this segregation should not extend beyond dimers. One may thus describe superconducting B-doped diamond as a random distribution of isolated impurities plus dimers in significant proportion. The effect of randomness is expected to average over the energies provided in the table.

C. Electronic properties

In order to understand the influence of dimerization on the superconducting transition, we now study the electronic properties associated with the configurations relaxed above. We reproduce in Fig. 1(a) the band structure associated with "isolated impurities" (3NN configuration) in the C_{54} cell. It is clearly similar to what was observed previously within supercell approaches with one B atom per cell.[17] Namely, the diamond band structure is essentially preserved close to the Fermi level (E_F) but with a slightly larger splitting of the $\Gamma_{25'}$ state in the present 3NN-B_2C_{52} cell due to larger symmetry breaking. This splitting ($\sim$150 meV) translates into a broadening of the valence band maximum (VBM) upon introduction of a true disorder within, e.g., the theoretical CPA approach.[19]

The situation changes significantly when one consider in Figs. 1(b)–1(d) the band structure associated with cells containing B dimers. The most striking result is the formation of a B-dimer-related impurity band centered 0.5 eV to 1 eV above the VBM. Such results might clearly explain the recent B-K XAS spectra reported by Nakamura *et al.*[25] showing the appearance in superconducting samples of broad unoccupied structures in the band gap, an observation that cannot be explained by considering isolated B atoms either in the VCA,[14–16] supercell,[17,18] or the CPA (Ref. 19) approaches. Such conclusions are consistent with the recent work by Goss and Briddon[40] showing in the more dilute limit (1 dimer per 256-atom cell) that B dimers yield deeper in-gap states than isolated boron in substitution. The in-gap band is highly dispersive and, in the NN-B_2C_{52} case, crosses the Fermi level around the **L** point. We believe, however, that this novel structure at E_F in an artifact of the supercell approach and that with disorder, a correct picture is that of a broad empty structure centered above the VBM. The most recent experimental angle resolved photoemission mapping of the occupied bands[11] suggests that there are no occupied bands crossing E_F away from zone center. Whether or not the dimer impurity band, or impurity states, overlap with the top of the valence bands in the limit of large dopant concentration, boron dimers yield empty states located well above the Fermi level.

An important consequence of the split off of an empty band from the VBM is that boron dimers are electrically inactive and will not contribute to the density of states at E_F as the B-induced holes are trapped by the in-gap empty band above the VBM. This is clearly demonstrated in the case of the NN-B_2C_{52} cell [Fig. 1(b)] which yields much less holes (as compared to the 3NN-B_2C_{52} cell) at the valence band maximum in Γ, and in the NN-B_2C_{62} cell [Fig. 1(c)], where the Fermi level is located above the VBM, as a consequence of the specific distribution of dimers, despite its $\sim$3% boron content. In a more realistic situation where isolated and dimerized boron atoms coexist, as in the NN-B_3C_{62} cell [Fig. 1(d)], only the isolated impurities will contribute to the hole density of states at the Fermi level. In particular, an increase in the boron concentration may not result in a straightforward manner in an increase of T_C as the relationship between boron and hole concentration at E_F is strongly affected by the presence of dimers. We will come back to that point in Sec. IV.

D. Phonon modes

We now study the zone-center phonon modes and the electron-phonon coupling. The analysis of the phonon eigenvectors associated with the B_2C_{52}-NN cell reveal several B-dimer related vibrational features, including two Raman

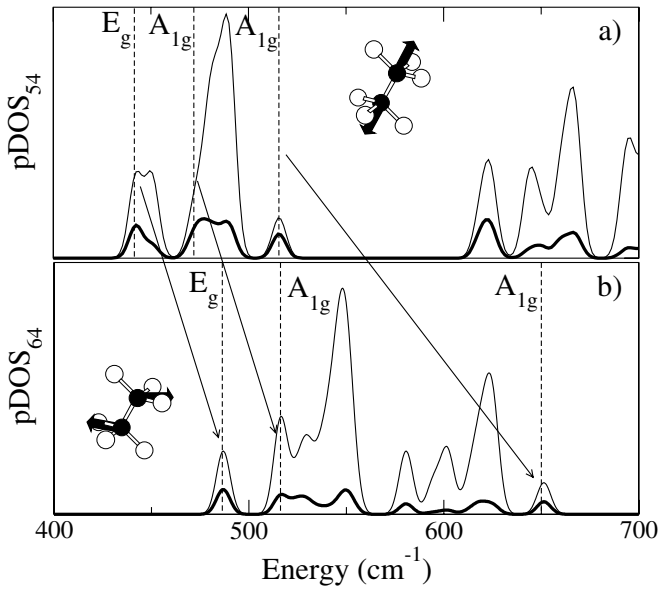

FIG. 2. Phonon density of states (pDOS) at $\mathbf{q}=\Gamma$ for (a) the B_2C_{52}-NN cell and (b) the B_2C_{62}-NN cell, restricted to the 400–700 cm^{-1} energy range. In thick line, the weight of the corresponding eigenmodes on the two B atoms and their six neighboring carbon atoms. Insets: schematic representation of (a) the A_{1g} B-B stretching modes and (b) the E_g wagging mode (B atoms in black).

active A_{1g} modes at 472 and 516 cm^{-1} and an E_g Raman active mode at 442 cm^{-1} (see Fig. 2). At high energy, an IR active E_u mode at 1350 cm^{-1} is also found to be very localized on the B dimer. The A_{1g} modes are associated with {111} stretching B motions, while E_g is a wagging mode (see the insets in Fig. 2). While the two A_{1g} modes are very similar with respect to the B atoms motions, they differ by the displacement of the backbonded carbon atoms. Similar results are obtained in the larger B_2C_{62}-NN cell but with a blueshift to 517 and 640 cm^{-1} for the A_{1g} modes, 486 cm^{-1} for the E_g mode, and 1362 cm^{-1} for the E_u mode. These variations indicate that the B-dimer vibrational modes are rather sensitive to the chemical environment in this large doping limit,[41] indicating that upon disorder such modes should yield a rather broad feature in the 450–550 cm^{-1} range. The present results confirm the preliminary work of Goss *et al.* in Ref. 36 providing "some evidence" of dimer-related vibrational structure in the 400–600 cm^{-1} range even though the method (combination of *ab initio* and valence force field) was considered by the authors not accurate enough to be precise.

E. Electron-phonon coupling

We finally study the influence of these B-related vibrational modes onto the electron-phonon coupling (and thus the superconducting transition temperature). A convenient energy-resolved representation of the strength of the electron-phonon coupling is the Eliashberg function. As in hole-doped diamond most of the coupling originates in zone-center modes, and in order to compare the theoretical results with the following Raman spectra, we focus on the restriction of the Eliashberg function to Brillouin zone center

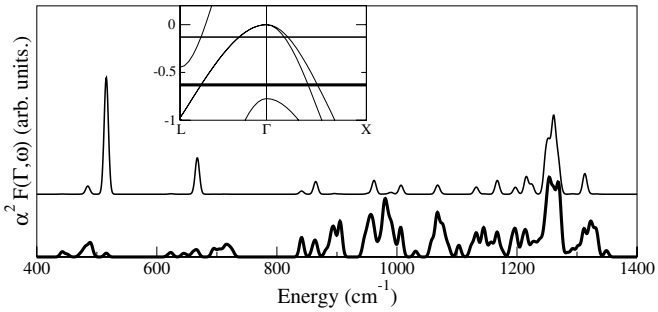

FIG. 3. (Upper thin line) Zone-center restricted Eliashberg function $\alpha^2F(\Gamma,\omega)$ for the B_2C_{52}-NN cell. (Lower thick line) $\alpha^2F(\Gamma,\omega)$ assuming that the Fermi level is located below the bottom of the dimer band (see text) at *L*. (Inset: detail of the valence band structure close to the valence band maximum at Γ. The thickness of the horizontal line representing the Fermi level corresponds to the line thickness of the Eliashberg function.)

phonons with the notation $\alpha^2F(\Gamma,\omega)$.[42] The Eliashberg function for the B_2C_{52}-NN cell is represented in Fig. 3. Associated with the thin line (upper graph), the Eliashberg function associated with the neutral B-dimer cell where the dimer-impurity band goes below the Fermi level (see band structure Fig. 1(b) and Fig. 3, inset) is represented. An analysis of the results indicates that, as expected, high-energy optical modes strongly contribute to the electron-phonon coupling. This is now well documented. More surprising is the strong contribution from the A_{1g} mode at 516 cm^{-1} which seems to indicate that boron dimer related modes may significantly contribute to the electron-phonon coupling. However, an analysis of the electronic states contributing to the peak in the Eliashberg function around 500 cm^{-1} clearly indicates that it is only the bottom of the dimer band at **L** that contributes to the coupling. By removing the contribution from the **L** point, which can be done by shifting the Fermi level just below the dimer band (see inset, Fig 3), the contribution from the dimer modes completely collapses (lower thick line in Fig. 3). This indicates that the dimer-related phonon modes do not couple to the hole states at the top of the valence band at Γ.

To confirm this absence of coupling, we study the evolution of the band structure upon a displacement of the atoms in the unit cell according to the phonon modes eigenvectors. In Figs. 1(b) and 1(c), the band structure upon activation of the A_{1g} mode at 516 and 640 cm^{-1} in the B_2C_{52}-NN and B_2C_{62} cell, respectively, are represented in dotted lines. Very clearly, the impurity dimer band is strongly affected by such phonons modes while the top of the valence band at Γ is nearly undistinguishable from the unperturbed lattice band structure. This confirms that the dimer-related Raman active modes around 500 cm^{-1} strongly couple with the unoccupied dimer band, but do not couple to the hole at zone center. In other words, the dimer vibrational modes will not contribute to the electron-phonon coupling responsible for the superconducting transition in B-doped diamond. The strong coupling to the dimer empty bands, and the lack of coupling with the hole states at Γ, can be rationalized by emphasizing that as the B-dimer band is deep into the gap, there is much less hybridization between boron and carbon bulk states as

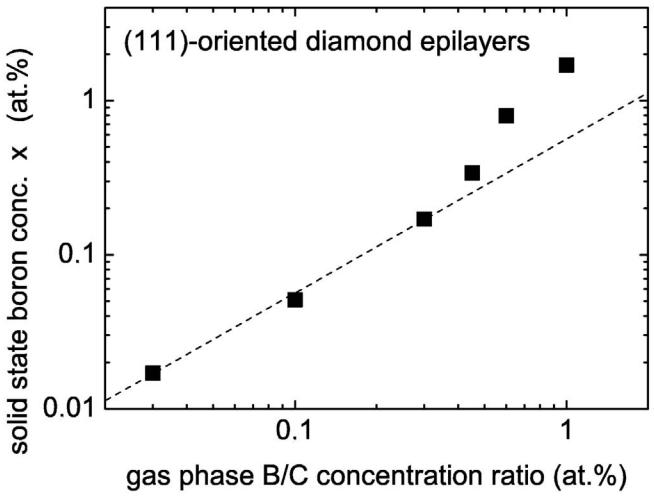

FIG. 4. SIMS measurement of the solid state incorporation of boron during (111)-oriented homoepitaxial growth. As a guide to the eyes, the doted line is the first diagonal with a slope of 1 (log-log scale).

compared to the standard degenerate semiconductor picture.

III. RAMAN MEASUREMENTS ON DOPED DIAMOND

To corroborate these theoretical findings, we now perform secondary ion mass spectroscopy (SIMS) and Raman measurements to study the structural and vibrational properties of normal and superconducting B-doped single crystal diamond. The critical temperatures quoted below were deduced from four point ac resistivity measurements and correspond to the temperature T_C at which the resistance is reduced to 90% of its normal state value.

A. Synthesis

The epilayers have been grown on commercial (001)- and (111)-oriented polished type Ib diamond substrates in a fused silica vertical microwave plasma-enhanced chemical vapor deposition reactor around 830 °C under a total pressure of 30 Torr [(001)-oriented growth] and at 890 °C under 50 Torr [growth along (111)]. Prior to deposition on a chemically cleaned surface, hydrogen was introduced in the reactor and the plasma was ignited. After several minutes, methane was introduced and a 200–500 nm thick buffer layer of nominally undoped material was deposited before the diborane was introduced. Methane was diluted 4 and 0.15% in hydrogen for (001)- and (111)-oriented growth, respectively, and the boron to carbon atomic concentration ratio in the gas phase was in the 500 to 2200 ppm range [growth along (001)] and between 300 and 10 000 ppm [for (111)-oriented growth]. The resulting deposition rates were around 1 μm/h along (001) and decreasing from 0.7 to 0.1 μm/h in the case of (111) oriented growth, while typical thicknesses were in the 0.3–3 μm range. The boron to carbon atomic ratio x has been deduced from calibrated secondary ion mass spectrometry profiles as described elsewhere.[4,43]

B. SIMS study of boron incorporation

An information on the incorporation of boron in diamond can be obtained by SIMS experiment. As shown in the log-log plot of Fig. 4, the solid state incorporation of boron during (111)-oriented homoepitaxial growth measured by SIMS was found to depart around $x=0.2$ at. % from its linear dependence on the boron to carbon atomic concentration in the gas mixture, to become significantly larger at higher concentrations. This change indicates that the mechanism for boron incorporation changes with concentration, and that some new reaction appears above $x=0.2\%$ which involves strong boron-boron correlations and a "larger than first-order" kinetic process. We propose to relate these changes to the calculations presented in Sec. II B, and shall consider this observation as an indication for the frequent occurrence of boron dimers in p-doped conditions (formation of dimers only would yield a slope of 2 in Fig. 4). Although the present (111) particular growth direction has been proposed to be particularly favorable to the incorporation of B-B pairs,[7] a similar departure from linearity has been also reported for the same concentration range in the case of (001)-oriented epitaxy.[44]

C. Raman measurements

In the spirit of the calculations presented, we shall now test whether the vibrational modes always present at 500 cm^{-1} in superconducting diamond are coupled to free carriers or not. To this end, micro-Raman backscattering studies have been performed at room temperature using either a HeCd cw laser (UV: 325 nm line) and a $\times 40$ objective or a HeNe cw laser (visible: 632.8 nm) and a $\times 100$ objective under confocal conditions. The spectral resolution was about 5 cm^{-1} in the UV and 2 cm^{-1} in the visible. The filtered scattered light was not analyzed for polarization but the respective configuration of the lasers and gratings led to a mostly parallel scattering geometry. The signal was collected by a liquid-nitrogen-cooled CCD detector over typical accumulation times on the order of an hour per spectral window.

Figure 5 shows the Raman spectra (Stokes) obtained under UV and visible light excitation on a heavily boron-doped diamond epilayer grown on a (001)-oriented substrate which became superconducting below 3.2 K. The lower spectrum, typical of many results previously obtained in the visible,[44,45] displays on a log scale a broad but pronounced and not quite symmetric peak around 500 cm^{-1}, a second weaker feature around 1000 cm^{-1}, an asymmetric band around 1230 cm^{-1}, a much narrower peak around 1315 cm^{-1} and then a strongly asymmetric dip around 1350 cm^{-1} on top of a slowly decreasing background. This dip is typical of a Fano line shape arising from the interference between the electronic scattering channels and the scattering by phonons corresponding to an ideally discrete vibronic energy level. Clearly, neither of the strongly parallel-polarized[44] (Γ_1 symmetry) broad peaks at 1000 cm^{-1} and 500 cm^{-1} are involved in this interference. This is a clear indication that, as compared to the softened zone-center optical modes at 1315 cm^{-1}, the vibrational modes in the 500 cm^{-1} energy range hardly couple to the electronic degrees of freedom.

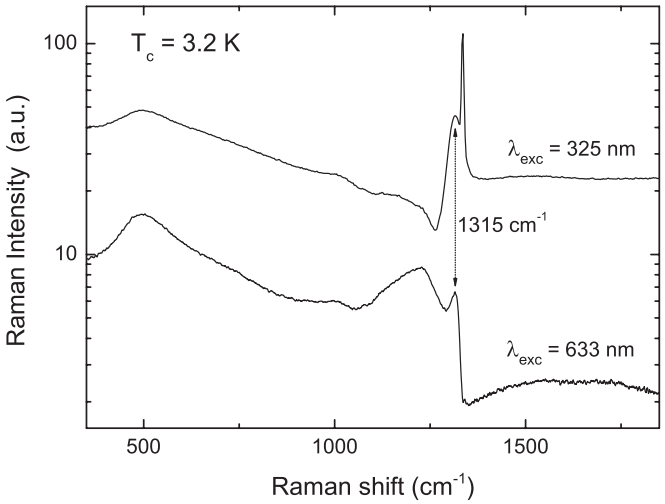

FIG. 5. Room temperature Raman backscattering spectra of a heavily B-doped diamond (001)-oriented epilayer displaying superconductivity below T_C=3.2 K. Two different excitation wavelengths have been used.

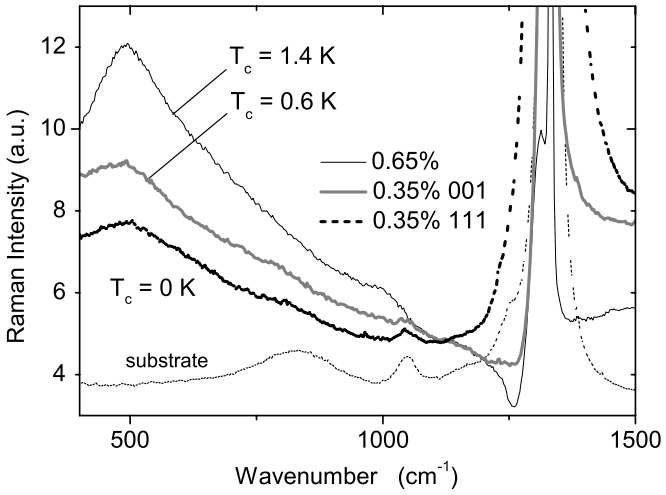

FIG. 6. Raman spectra of normal and superconducting diamond as a function of T_C.

In the spectrum obtained with an UV excitation at a nearly double frequency where the electronic scattering events become quite rare, the electronic scattering tail seems absent and the Fano antiresonance dip lies at 1270 cm^{-1}, below the softened zone-center peak observed at the same 1315 cm^{-1} wave number as for a visible light excitation. This peak is flanked by a resolution-limited line showing up at 1332 cm^{-1}, attributed to the optical phonon of undoped diamond. The 1230 cm^{-1} band appears as a mere modulation on the low-wave-number side of the Fano-related narrow dip. Slightly broader than their counterparts measured in the visible, both the 1000 and 500 cm^{-1} features are also present in this UV-excited spectrum. Again here, neither of these peaks are affected by the presence of free carriers.

Based on the above-described supercell calculations and on the experimentally observed absence of electron-phonon coupling, we attribute the polarized Raman broad peak observed around 500 cm^{-1} to the Raman active A_1 stretching modes of B-B dimers, and the 1000 cm^{-1} satellite to their first harmonic. The same assignment of the spectral feature at 500 cm^{-1} has also been suggested recently by other experimentalists[46] on the basis of preliminary calculations of the local vibrational modes of B_nH_n defects in diamond[36] based on a less accurate combined semiempirical *ab initio* calculation. Although a direct proof such as that provided by isotopic substitution studies is still lacking, the fact that in Fig. 5 these features remain quite unaffected by very different excitation conditions indicates that they do not have an electronic origin and that the Raman-active phonons they originate from are not strongly coupled to free carriers.

Additional evidence of this assignment and of the weak coupling is provided by Fig. 6 where we compare Raman spectra obtained in the UV range on a type Ib diamond substrate and on various heavily B-doped homoepitaxial films: the broad peak is clearly observed around 500 cm^{-1} in a (111)-oriented sample which is insulating at low temperature (T_C=0 K) and does not yield the Fano-related dip around 1270 cm^{-1} despite its relatively high boron content (x =0.35 at. %). In the case of (001)-oriented growth, only the samples displaying the 500 and 1000 cm^{-1} peaks, the bump around 1230 cm^{-1} and the Fano-related dip around 1270 cm^{-1} were found to become superconducting. As illustrated by Fig. 6, this peak became narrower, stronger and slightly shifted to lower wave numbers as the doping and resulting T_C was increased, while the Fano-related bump-and-dip feature around 1250 cm^{-1} became more obvious. This dip in the UV-excited Raman spectrum is thus the clearest spectroscopic token of the metallic character (in the normal state) of the boron-doped diamond epilayers which become superconducting at low temperatures.

The insulating character (at low temperatures) of the present (111)-oriented epilayer with x=0.35 at. %, which is reminiscent of our insulating B_2C_{62}-NN cell, indicates that compensating defects and/or nondoping boron atoms occur in a sizable proportion when growth is along this direction under our low methane concentration (0.15%) deposition conditions. This behavior, where the T_C of (111)-oriented epilayer is much lower than that of a layer grown along (001) with the same boron content, is in contrast to that observed in recent reports[7,10] about films with a much higher T_C grown at higher methane concentrations, a fact which deserves further investigation.

IV. DISCUSSION

The present theoretical and experimental findings, confirming early work on the possible occurrence of boron dimers[36,40] in B-doped diamond, clearly suggest that one should not expect a simple dependence of the free carrier concentration at E_F, and thus of T_C, on the boron content. In particular, we believe that the difficulties in relating the boron content to T_C in a universal and straightforward manner should not be taken as evidence for deviations from a standard BCS picture as suggested in Ref. 8.

These conclusions on the segregation of boron in dimers are based on thermodynamical (energetical) considerations.

Diffusion processes (kinetics) in bulk samples are limited by the large diffusion barrier of substitutional boron atoms.[40] Such large barriers may not apply during growth where B atoms are expected to diffuse more easily at surfaces. The important role of surface processes in the incorporation of boron dimers is strongly supported by the present results (see Fig. 6) and that of Ref. 7 clearly showing that, depending on the crystallographic direction of growth, samples with equivalent B content may exhibit very different T_C, corresponding to a different doping efficiency of boron impurities.

Our results do not rule out the existence of other type of defects generating empty states in the band gap and/or specific vibrational modes. Preliminary results indicate that interstitial boron generates two bands deep into the gap and several B-related vibrational modes at low energy (370–450 cm^{-1}) and three very localized high energy modes at 1625, 1630, and 1900 cm^{-1} (54 atoms cell), a situation reminiscent of the nitrogen interstitial.[47] Clearly, the presence of high-energy infrared active modes (much higher than the B-dimer E_u mode) might be used as a signature of the interstitial in future experimental studies. However, as emphasized by Goss and Briddon in Ref. 40, the high formation energy of such a defect do not play in favor of the presence of a large number of interstitials that could explain the very strong Raman peak at about 500 cm^{-1} in superconducting samples. This contrasts significantly with the present case of dimers that are strongly favored in hole-doping conditions. Further, it is difficult to understand how the larger-than-one order in the kinetic of boron incorporation, observed in SIMS measurements (Fig. 4), could be explained by the formation of isolated interstitial boron atoms.

It was suggested in a previous supercell theoretical study[18] performed on a small $2\times2\times2$ cell (6.25% B concentrations), that high boron content may lead to "softened" B-C stretching modes in the 500–600 cm^{-1} energy range. We do find similar results in the case of our B_2C_{52}-3NN cell. We observe however, and as in Ref. 18, that such modes contribute significantly to the electron-phonon coupling, a result which is not consistent with the present experimental Raman study. Of course, isolated boron atoms, possibly generating softened modes in the 500–600 cm^{-1} energy range, will coexist with dimer modes, contributing to the broad low energy Raman active structure.

The present theoretical results are based on supercell (periodic) approaches where disorder cannot be fully described. Future calculations within, e.g., the CPA approach,[19] with a disorder biased towards the preferential formation of dimers, may be performed in order to get more insight into the electronic properties of a random distribution of dimers and isolated B atoms. Unfortunately, the calculation of the vibrational modes, and of the electron-phonon coupling, is far from being a trivial task within this approach. From an experimental point of view, isotopic substitutions will probably be necessary to confirm the role of boron dimers, as well as EXAFS or NMR studies, coupled to Hall effect measurements.

V. CONCLUSIONS

We have studied both theoretically and experimentally the effect of impurity clustering in superconducting diamond. Total energy calculations for various neutral and charged defect structures suggest that a significant fraction of boron atoms may form B dimers, a conclusion corroborated by SIMS measurements. The calculated vibrational modes associated with dimers are found to yield several Raman active modes in the 400–600 cm^{-1} energy range, in excellent agreement with experimental Raman measurements evidencing the appearance upon increasing doping of a broad Raman active peak around 500 cm^{-1}. Segregation into clusters larger than dimers is not expected. It is found that B dimers should not contribute to the enhancement of T_C as they yield electrically inactive empty states in the band gap and vibrational modes that do not couple to the electronic states close to the zone-center states around E_F. These finding bear important consequences on the evolution of T_C with increasing doping concentration.

ACKNOWLEDGMENTS

Calculations have been performed at the French CNRS national computer center at IDRIS (Orsay). The authors acknowledge support from ANR "SupraDiam" GRANT No. NT05-1_41912.

[1] M. Cohen, Rev. Mod. Phys. **36**, 240 (1964).
[2] E. A. Ekimov, V. A. Sidorov, E. D. Bauer, N. N. Mel'nik, N. J. Curro, J. D. Thompson, and S. M. Stishov, Nature (London) **428**, 542 (2004).
[3] Y. Takano, M. Nagao, I. Sakaguchi, M. Tachiki, T. Hatano, K. Kobayashi, H. Umezawa, and H. Kawarada, Appl. Phys. Lett. **85**, 2851 (2004).
[4] E. Bustarret, J. Kačmarčik, C. Marcenat, E. Gheeraert, C. Cytermann, J. Marcus, and T. Klein, Phys. Rev. Lett. **93**, 237005 (2004).
[5] V. A. Sidorov, E. A. Ekimov, S. M. Stishov, E. D. Bauer, and J. D. Thompson, Phys. Rev. B **71**, 060502(R) (2005).
[6] J. Kačmarčik, C. Marcenat, C. Cytermann, A. Ferreira da Silva, L. Ortega, F. Gustafsson, J. Marcus, T. Klein, E. Gheeraert, and E. Bustarret, Phys. Status Solidi A **202**, 2160 (2005).
[7] H. Umezawa, T. Takenouchi, Y. Takano, K. Kobayashi, M. Nagao, I. Sakaguchi, M. Tachiki, T. Hatano, G. Zhong, M. Tachiki, and H. Kawarada, cond-mat/0503303 (unpublished).
[8] K. Winzer, D. Bogdanov, and Ch. Wild, Physica C **432**, 65 (2005).
[9] Z. I. Wang, Q. Luo, L. W. Liu, C. Y. Li, H. X. Yang, H. F. Yang, J. J. Li, X. Y. Lu, Z. S. Jin, L. Lu, and C. Z. Gu, Diamond Relat. Mater. **15**, 659 (2006).
[10] T. Takenouchi and H. Kawarada (private communication).
[11] T. Yokoya, T. Nakamura, T. Matsushita, T. Muro, Y. Takano, M. Nagao, T. Takenouchi, H. Kawarada, and T. Oguchi, Nature

(London) **438**, 647 (2005).
[12] B. Sacépé, C. Chapelier, C. Marcenat, J. Kačmarčik, T. Klein, M. Bernard, and E. Bustarret, Phys. Rev. Lett. **96**, 097006 (2006).
[13] M. Ortolani, S. Lupi, L. Baldassarre, P. Calvani, U. Schade, Y. Takano, M. Nagao, T. Takenouchi, and H. Kawarada, cond-mat/0602150 (unpublished).
[14] K. W. Lee and W. E. Pickett, Phys. Rev. Lett. **93**, 237003 (2004).
[15] L. Boeri, J. Kortus, and O. K. Andersen, Phys. Rev. Lett. **93**, 237002 (2004).
[16] Y. Ma, J. S. Tse, T. Cui, D. D. Klug, L. Zhang, Y. Xie, Y. Niu, and G. Zou, Phys. Rev. B **72**, 014306 (2005).
[17] X. Blase, Ch. Adessi, and D. Connétable, Phys. Rev. Lett. **93**, 237004 (2004).
[18] H. J. Xiang, Z. Li, J. Yang, J. G. Hou, and Q. Zhu, Phys. Rev. B **70**, 212504 (2004).
[19] K.-W. Lee and W. E. Pickett, Phys. Rev. B **73**, 075105 (2006).
[20] J. Chevallier, B. Theys, A. Lusson, C. Grattepain, A. Deneuville, and E. Gheeraert, Phys. Rev. B **58**, 7966 (1998).
[21] V. A. Sidorov, E. A. Ekimov, E. D. Bauer, N. N. Mel'nik, N. J. Curro, V. Fritsch, J. D. Thompson, S. M. Stishov, A. E. Alexenko, and B. V. Spitsyn, Diamond Relat. Mater. **14**, 335 (2005).
[22] J. Nagamatsu, N. Nakagawa, T. Muranaka, Y. Zenitani, and J. Akimitsu, Nature (London) **410**, 63 (2001).
[23] H. Kawaji, H. O. Horie, S. Yamanaka, and M. Ishikawa, Phys. Rev. Lett. **74**, 1427 (1995); K. Tanigaki, T. Shimizu, K. M. Itoh, J. Teraoka, Y. Moritomo, and S. Yamanaka, Nat. Mater. **2**, 653 (2003); D. Connétable, V. Timoshevskii, B. Masenelli, J. Beille, J. Marcus, B. Barbara, A. M. Saitta, G.-M. Rignanese, P. Mélinon, S. Yamanaka, and X. Blase, Phys. Rev. Lett. **91**, 247001 (2003).
[24] A. Floris, G. Profeta, N. N. Lathiotakis, M. Lüders, M. A. L. Marques, C. Franchini, E. K. U. Gross, A. Continenza, and S. Massidda, Phys. Rev. Lett. **94**, 037004 (2005).
[25] J. Nakamura, T. Oguchi, N. Yamada, K. Kuroki, K. Okada, Y. Takano, M. Nagao, I. Sakaguchi, H. Kawarada, R. C. C. Perera, and D. L. Ederer, cond-mat/04010144 (unpublished).
[26] J. Nakamura, E. Kabasawa, N. Yamada, Y. Einaga, D. Saito, H. Isshiki, S. Yugo, and R. C. C. Perera, Phys. Rev. B **70**, 245111 (2004).
[27] Yu. G. Pogorelov and V. M. Loktev, Phys. Rev. B **72**, 075213 (2005).
[28] G. Baskaran, cond-mat/0404286 (unpublished); cond-mat/O410296 (unpublished).
[29] D. Wu, Y. C. Ma, Z. L. Wang, Q. Luo, C. Z. Gu, N. L. Wang, C. Y. Li, X. Y. Lu, and Z. S. Jin, Phys. Rev. B **73**, 012501 (2006).
[30] J. P. Perdew, K. Burke, and M. Ernzerhof, Phys. Rev. Lett. **77**, 3865 (1996).
[31] P. Hohenberg and W. Kohn, Phys. Rev. **136**, B864 (1964); W. Kohn and L. J. Sham, Phys. Rev. **140**, A1133 (1965).
[32] S. Baroni, S. de Gironcoli, A. Dal Corso, and P. Giannozzi, Rev. Mod. Phys. **73**, 515 (2001); S. Baroni, A. Dal Corso, S. de Gironcoli, and P. Giannozzi, http://www.pwscf.org
[33] N. Troullier and J. L. Martins, Phys. Rev. B **43**, 1993 (1991).
[34] A. M. Rappe, K. M. Rabe, E. Kaxiras, and J. D. Joannopoulos, Phys. Rev. B **41**, 1227 (1990); K. Laasonen, R. Car, C. Lee, and D. Vanderbilt, *ibid.* **43**, 6796 (1991).
[35] Jun Yamauchi, N. Aoki, and I. Mizushima, Phys. Rev. B **63**, 073202 (2001).
[36] J. P. Goss, P. R. Briddon, R. Jones, Z. Teukam, D. Ballutaud, F. Jomard, J. Chevallier, M. Bernard, and A. Deneuville, Phys. Rev. B **68**, 235209 (2003).
[37] We have tested a few configurations for the B_3C_{61} systems where a dimer coexists with a hole-donating isolated boron atom, providing thus a more realistic description of dimers in hole-doping conditions. Again within LDA, the dimer configurations were found to be more stable than those where B atoms are "isolated," with energies ranging from 50 to 300 meV. However, the very large number of nonequivalent configurations associated with three boron atoms does not allow for a systematic study of the relative energy of dimerized versus fully segregated topologies.
[38] As shown below, a distribution of neutral B dimers yields hardly any hole at the top of the valence band maximum (VBM) in Γ, a situation that contrasts with the experimental observations performed on heavily *p*-doped diamond.
[39] In this approach, the added charge is neutralized by a jellium background of opposite sign. For a recent analysis of the study of "charged states" with supercell techniques, see J. Shim, E.-K. Lee, Y. J. Lee, and R. M. Nieminen, Phys. Rev. B **71**, 245204 (2005).
[40] J. P. Goss and P. R. Briddon, Phys. Rev. B **73**, 085204 (2006).
[41] We note that the phonons corresponding to the B_2C_{62}-NN cell are calculated for an insulating structure (see text), while in the B_2C_{52}-NN cell the Fermi level is located below the valence band maximum. We expect that upon additional hole-doping, the modes associated with the B_2C_{62}-NN should be somehow softened, reducing the frequency differences between the two cells.
[42] We recall that the zone-center phonons of the $(3\times3\times3)$ supercell includes, by band folding, all modes with momentum on a $(3\times3\times3)$ grid sampling the Brillouin zone of the "conventional" irreducible two-atom cell.
[43] C. Tavares, F. Omnès, J. Pernot, and E. Bustarret, Diamond Relat. Mater. **15**, 582 (2006); M. Mermoux, F. Jomard, C. Tavares, F. Omnès, and E. Bustarret, *ibid.* **15**, 572 (2006).
[44] E. Bustarret, A. Gheeraert, and K. Watanabe, Phys. Status Solidi A **199**, 9 (2003).
[45] F. Pruvost, E. Bustarret, and A. Deneuville, Diamond Relat. Mater. **9**, 295 (2000).
[46] M. Bernard, C. Baron, and A. Deneuville, Diamond Relat. Mater. **13**, 896 (2004).
[47] J. P. Goss, P. R. Briddon, S. Papagiannidis, and R. Jones, Phys. Rev. B **70**, 235208 (2004).